Cdc42 antagonizes Rho1 activity at adherens junctions to limit epithelial cell apical tension

Stephen J. Warner[1,2] and Gregory D. Longmore[1,2]

[1]Department of Medicine and [2]Department of Cell Biology and Physiology, Washington University, St. Louis, MO 63110

In epithelia, cells are arranged in an orderly pattern with a defined orientation and shape. Cadherin containing apical adherens junctions (AJs) and the associated actomyosin cytoskeleton likely contribute to epithelial cell shape by providing apical tension. The Rho guanosine triphosphatases are well known regulators of cell junction formation, maintenance, and function. Specifically, Rho promotes actomyosin activity and cell contractility; however, what controls and localizes this Rho activity as epithelia remodel is unresolved. Using mosaic clonal analysis in the *Drosophila melanogaster* pupal eye, we find that Cdc42 is critical for limiting apical cell tension by antagonizing Rho activity at AJs. Cdc42 localizes Par6–atypical protein kinase C (aPKC) to AJs, where this complex limits Rho1 activity and thus actomyosin contractility, independent of its effects on Wiskott-Aldrich syndrome protein and p21-activated kinase. Thus, in addition to its role in the establishment and maintenance of apical–basal polarity in forming epithelia, the Cdc42–Par6–aPKC polarity complex is required to limit Rho activity at AJs and thus modulate apical tension so as to shape the final epithelium.

Introduction

Epithelial cells undergo dynamic changes in cell shape as epithelia undergo morphogenetic changes such as those that occur during normal development (Montell, 2008) and carcinoma invasion and metastasis, where aberrant epithelial cell contractility and morphology are present (Olson and Sahai, 2009). A critical determinant of cell morphology is the actomyosin cytoskeleton (Montell, 2008), and key regulators of this process are the family of Rho GTPases. Rho, in particular, directly controls actomyosin contractility by activating two specific effectors: Rho-associated kinase (Rok) to promote phosphorylation and activation of the myosin light chain (MLC) and Diaphanous (Dia) to promote actin filament assembly (Burridge and Wennerberg, 2004). However, how this Rho activity is localized to adherens junctions (AJs) and regulated during epithelial morphogenesis is not understood. Cdc42, another Rho GTPase, also influences cell morphology. Cdc42-null mouse embryonic fibroblasts have contracted cell bodies (Yang et al., 2006), and Cdc42 regulates *Drosophila melanogaster* dorsal thorax epithelial cell shape (Georgiou et al., 2008; Leibfried et al., 2008). Moreover, during some tumor cell line invasion in ex vivo cultures, Cdc42 cooperates with Rho to activate myosin and enhance mesenchymal cell motility (Wilkinson et al., 2005). Despite this, precisely how Cdc42 regulates epithelial cell shape during in vivo morphogenetic processes is not known.

The *Drosophila* pupal eye is a postmitotic nonproliferating, remodeling neuroepithelium amenable to in vivo clonal genetic loss-of-function (LOF) analyses. The *Drosophila* eye contains a hexagonal array of repeating functional units called ommatidia. Each ommatidium has a neuronal core of photoreceptors and cone cells surrounded by light-insulating pigment epithelial cells (PECs; Cagan and Ready, 1989). By 40 h after puparium formation (APF), the PECs form a highly predictable pattern with extreme fidelity, with each type of PEC (primary, secondary, and tertiary) having a precise morphology repeated across all ommatidia. This, in combination with the use of clonal analysis to genetically modify individual or groups of

The Rockefeller University Press $30.00
J. Cell Biol. Vol. 187 No. 1   119–133
www.jcb.org/cgi/doi/10.1083/jcb.200906047

JCB   **119**

cells within a tissue of otherwise wild-type (WT) cells, allows changes in PEC morphology to be easily detected, quantified, and structurally analyzed so as to identify and interrogate molecular pathways that regulate epithelial cell morphology.

The *Drosophila* pupal eye has been used to study other epithelial properties such as cell adhesion (Hayashi and Carthew, 2004; Bao and Cagan, 2005) and cell fate decisions (Nagaraj and Banerjee, 2007). Although PECs are all epithelial cells, these studies have revealed important differences between the three types of PECs. For example, two important adhesion molecules in PEC patterning, Roughest and Hibris, are expressed in complementary PECs, with Hibris expressed in primary PECs and Roughest in secondary and tertiary interommatidial precursor cells (Bao and Cagan, 2005).

The pupal eye also serves as a model of a mature epithelium with formed but remodeling intercellular junctions, as opposed to proliferating epithelia (*Drosophila* embryonic or larval tissue culture) with newly forming junctions between cells. Specifically, differences exist between how AJs are maintained and remodeled in the pupal eye epithelium, which is independent of the formin protein Dia (Warner and Longmore, 2009), compared with the establishment and maintenance of AJs in *Drosophila* embryo and mammalian tissue culture cells, which requires Dia (Sahai and Marshall, 2002; Kobielak et al., 2004; Homem and Peifer, 2008). In this study, we used the pupal eye to determine the function of the Rho GTPase Cdc42 in these nonproliferating, remodeling epithelial cells.

Results

Cdc42 regulates septate junction (SJ) organization but not AJs in nonproliferating, remodeling epithelia

To determine functions for Cdc42 in this nonproliferating yet remodeling epithelium in vivo, we performed mosaic analysis with a repressible cell marker (MARCM) clonal analysis (Lee and Luo, 1999) with a strong *Cdc42* LOF allele, *Cdc42⁴*, in *Drosophila* pupal eye PECs (Fig. 1, A and B). Considering Cdc42's well-described role in the establishment and possibly maintenance of epithelial apical–basal polarity and intercellular junctions, we first turned our attention to the possible effects of Cdc42 depletion on the organization and function of both AJs and SJs (the *Drosophila* functional homologue of vertebrate tight junctions; Furuse and Tsukita, 2006) and apical–basal polarity. Secondary and tertiary PECs clonal for *Cdc42⁴* had unchanged AJs and SJs, as determined by immunofluorescence for *Drosophila* epithelial cadherin (DE-cadherin) for AJs and Discs large (Dlg), Scribble (Scrib), or Coracle for SJs (Fig. 1, C, D, and F). However, in primary PECs, SJ-associated proteins but not AJ proteins were mislocalized (Fig. 1, C–G). This cell-selective effect of Cdc42 depletion on primary PEC SJs was specific, as expression of WT Cdc42 within *Cdc42⁴* clonal cells reverted the phenotype (Fig. 1 H and Table S1).

Studies of Rho GTPase function often use dominant-negative (DN) proteins to ascertain the effect of inhibiting specific Rho GTPase functions. Whether these manipulations are Rho GTPase type specific and mimic specific GTPase genetic depletion or deletion has not been directly established in most instances (Heasman and Ridley, 2008). Therefore, we compared pupal eye epithelium phenotypes from genetic depletion of Cdc42 with Cdc42-DN expression. Expression of DN Cdc42-N17 resulted in severe disruption of AJs mainly between secondary and tertiary PECs, whereas SJs remained intact (Fig. S3, A–C). In primary PECs, AJ and SJ organization was not affected (Fig. S3, B and C). These phenotypes were in stark contrast to Cdc42 LOF clones, which had no effect on AJs and mislocalization of primary PEC SJ proteins (Fig. 1, C–G). Even in large *Cdc42⁴* clones with more severe patterning defects, no AJ disruptions were seen (Fig. S3 D), indicating that differences between Cdc42-DN and LOF phenotypes were unlikely the result of Cdc42 protein perdurance in *Cdc42⁴* clones.

Although Cdc42 has been shown to be important for proper cell polarity in several mammalian and *Drosophila* cell types (Hutterer et al., 2004; Schwamborn and Püschel, 2004; Atwood et al., 2007; Martin-Belmonte et al., 2007), depletion of Cdc42 in pupal eye epithelia did not disrupt apical–basal polarity, as indicated by the persistent and appropriate apical localization of DE-cadherin in *Cdc42⁴* clonal PECs (Fig. 1, E′ and G′, confocal z projections). Cdc42 depletion also did not disrupt Crumbs (Crbs) membrane localization (Fig. S4, G–I).

The Dlg–Scrib–lethal (2) giant larvae complex is also important for apical–basal polarity establishment in mammalian and *Drosophila* epithelia (Bilder, 2004). Surprisingly, although depletion of Cdc42 in PECs disrupted Dlg and Scrib localization (Fig. 1, C, F, and G), epithelial polarity was unaffected (Fig. 1, E′ and G′). Even MARCM clones with a *dlg*-null allele, *dlg^M52^*, or a *scrib*-null allele, *scrib¹*, did not exhibit disruption of pupal eye PEC polarity (Fig. S1, A–C). Indeed depletion of both Dlg and Scrib, by expressing Dlg-RNAi in *scrib¹* MARCM clones did not alter normal apical–basal polarity (Fig. S1 D). These data indicated that, as opposed to their roles in the establishment and maintenance of polarity in proliferating epithelia (Bilder, 2004; Hutterer et al., 2004; Martin-Belmonte et al., 2007), Cdc42, Dlg, and Scrib were also not required for the maintenance of epithelial cell polarity in this nonproliferating epithelium.

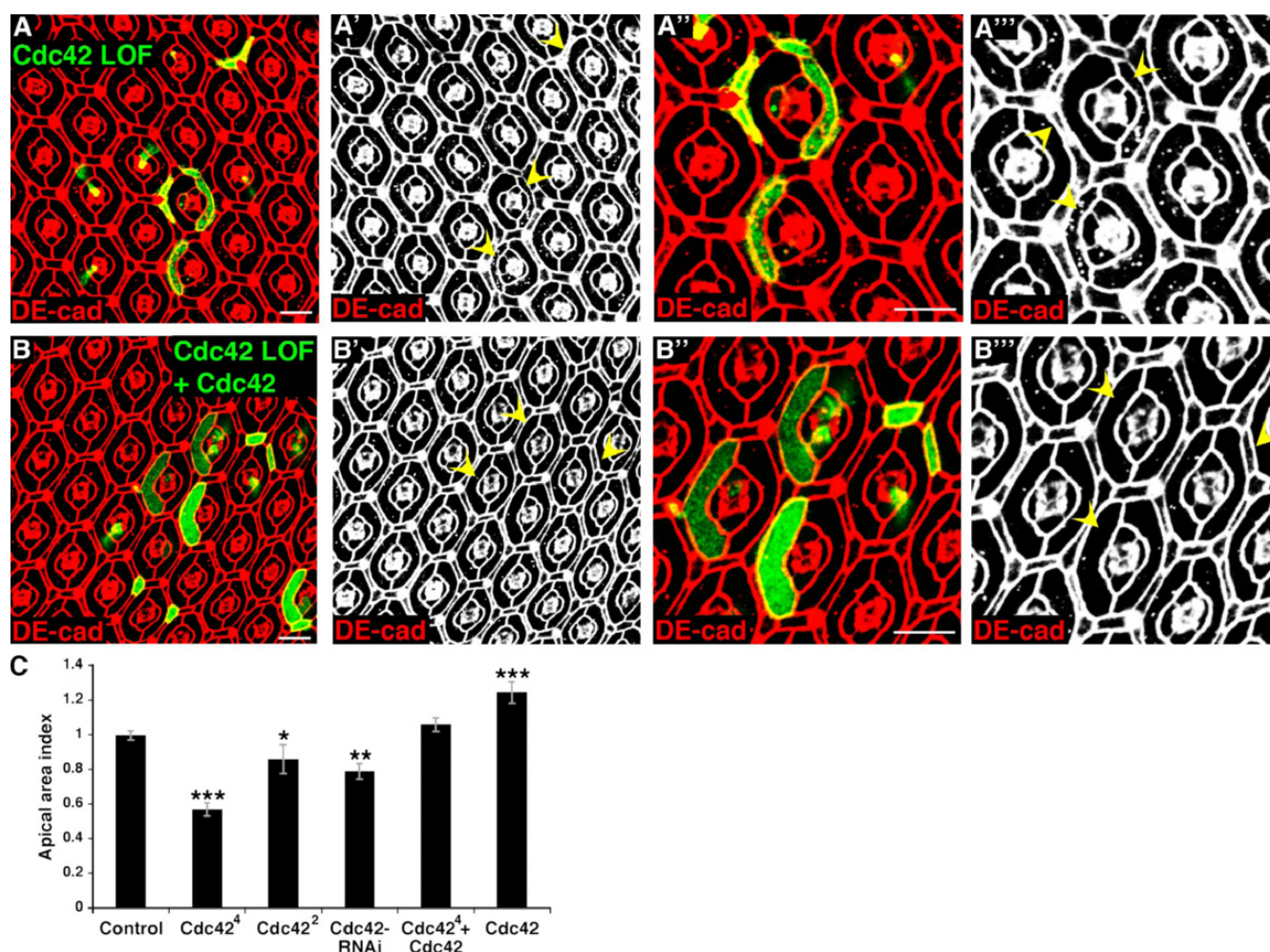### Cdc42 inhibits apical cell tension

Cdc42 is also known to regulate cell morphology, but precisely how is not clear. Consistent with previous studies (Georgiou et al., 2008; Leibfried et al., 2008), we found that all PECs depleted of Cdc42 had decreased apical cell area, as determined by the area outlined by DE-cadherin (Fig. 2, A and C; and Table S2). Analysis of single-cell PEC *Cdc42⁴* clones indicated that the decrease in apical area was cell autonomous and specific to the AJ level (Fig. 3, A and B; and Table S2). In WT PECs, the AJs and SJs were aligned along the apical–basal axis (Fig. 3, A and B, white asterisks); however, in *Cdc42⁴* PEC clones, AJs were spaced within the SJs (Fig. 3, A and B, yellow arrowheads and asterisks). Analysis basal to the SJs revealed no other significant changes in cell shape compared with surrounding cells (unpublished data). This decrease in apical cell area in *Cdc42⁴* clonal cells was rescued by expression of Cdc42 in *Cdc42⁴* clonal cells (Fig. 2, B and C). We also observed this phenotype
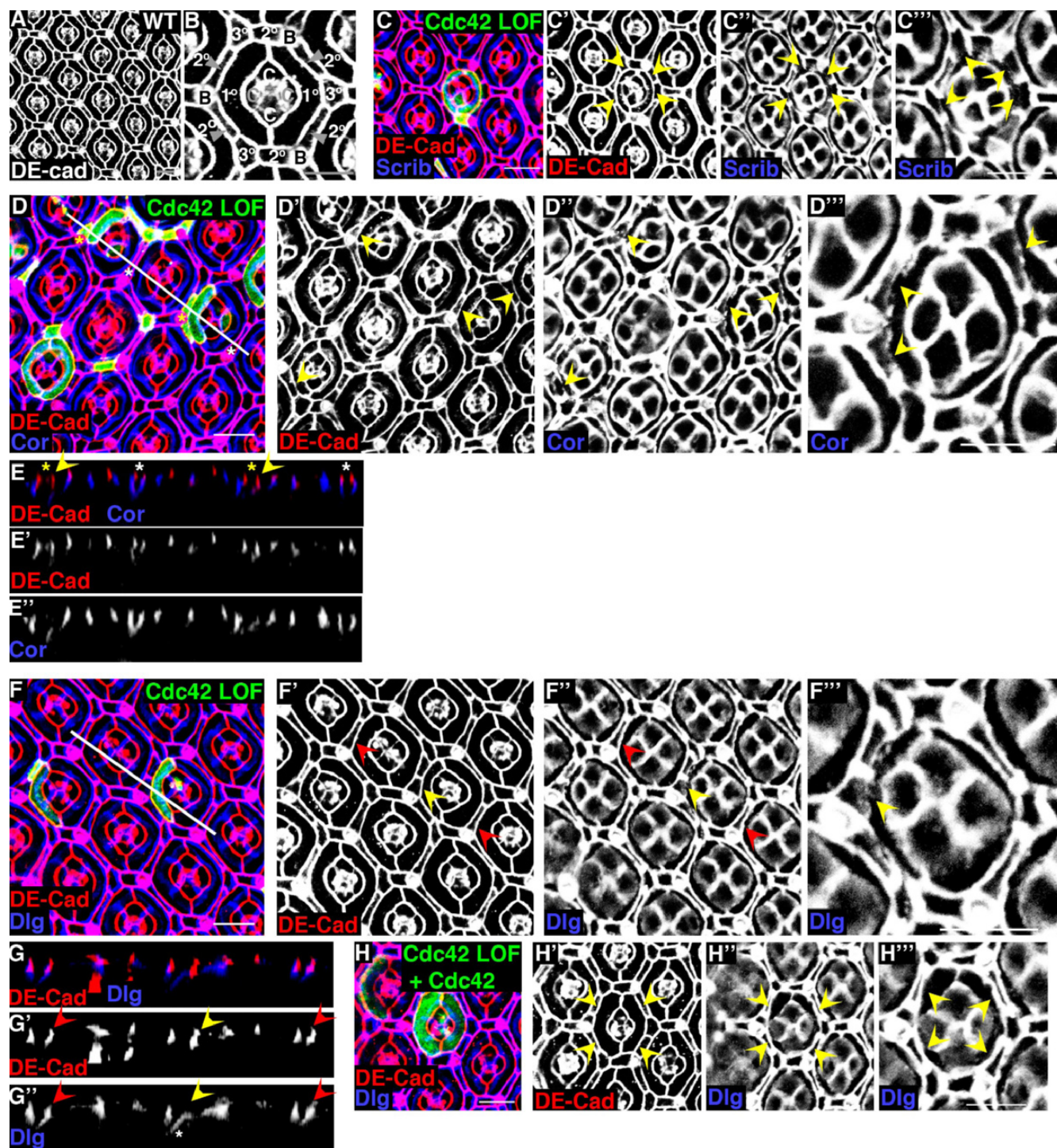
Figure 1. **Cdc42 regulates SJ organization but not AJs or apical–basal polarity.** (A and B) Confocal immunofluorescent localization of DE-cadherin (DE-Cad) in WT pupal eye. 1°, primary PEC; 2°, secondary PEC; 3°, tertiary PEC; B, bristle cell; C, cone cell. The photoreceptors are basal to this optical section. Anterior is to the right in all images. This and subsequent pupal eyes are 40 h APF. (C) Confocal immunofluorescent localization of DE-cadherin (C and C') and Scrib (C, C'', and C''') in *Cdc42⁴* MARCM clones. Arrowheads identify AJs (C') and SJs (C'' and C''') around *Cdc42⁴* clonal primary PECs. In this and subsequent images of AJs and SJs together, SJs were imaged ∼1 µm basal to the AJs. (D and E) Confocal immunofluorescent localization of DE-cadherin (D, D', E, and E') and Coracle (Cor; D, D''–E, and E'') in apical (D–D''') and lateral (E–E'') optical sections of *Cdc42⁴* MARCM clones. The white line (D) identifies where the lateral section (E–E'') was taken. Yellow asterisks identify *Cdc42⁴* MARCM clones, whereas white asterisks identify analogous nonclonal WT cells. Arrowheads identify AJs (D' and E) and SJs (D''–E) around *Cdc42⁴* clonal primary PECs. (F and G) Confocal immunofluorescent localization of DE-cadherin (F, F', G, and G') and Dlg (F, F''–G, and G'') in apical (F–F''') and lateral (G–G'') optical sections of *Cdc42⁴* MARCM clones. The white line (F) identifies where the lateral section (G–G'') was taken. Yellow arrowheads identify an AJ (F' and G') and SJ (F'', F''', and G'') around the *Cdc42⁴* clonal cell, whereas red arrowheads identify AJs (F' and G') and SJs (F'' and G'') around analogous nonclonal WT cells. The asterisk (G'') identifies a photoreceptor axon projecting through the ommatidium. (H) Confocal immunofluorescent localization of DE-cadherin (H and H') and Dlg (H, H'', and H''') in *Cdc42⁴* MARCM clones that express WT Cdc42. Arrowheads identify AJs (H') and SJs (H'' and H''') around clonal cells. Bars, 10 µm.

Figure 2. Cdc42 inhibits apical cell tension. (A) Confocal immunofluorescent localization of DE-cadherin (DE-cad) in *Cdc42[4]* MARCM clones. (B) Confocal immunofluorescent localization of DE-cadherin in *Cdc42[4]* MARCM clones expressing WT Cdc42. (A and B) Arrowheads identify clonal cells. (C) Quantification of apical areas in clonal cells depleted of Cdc42 or overexpressing WT Cdc42 (for apical area index, see Table S2). Data are represented as mean ± SD. *, $P < 0.05$; **, $P < 0.01$; ***, $P < 0.001$. Bars, 10 µm.

in MARCM clones with a weak *Cdc42* LOF allele, *Cdc42[2]*, and flippase (Flp)-out clones (Ito et al., 1997) with Cdc42-RNAi (Fig. 2 C, Fig. S2 A, and Table S2), although these manipulations decreased apical area to a lesser extent compared with the strong LOF allele *Cdc42[4]* (Fig. 2 C), likely reflecting the amount of residual Cdc42 protein. Moreover, overexpression of Cdc42 in PECs resulted in increased apical area at the AJ level (Figs. 2 C and 3 C and Table S2), and PECs overexpressing Cdc42 had AJs that were spaced wider than SJs (Fig. 3 C″, white arrowhead). Depletion of Cdc42 in the pupal wing epithelium, by expressing Cdc42-RNAi in a defined subset of cells, also resulted in decreased epithelial cell apical areas (Fig. S5, F and G). Together, these data indicated that Cdc42 contributes to epithelial cell shape possibly by limiting apical tension of pupal epithelial cells. Unlike Cdc42, MARCM clones null for *rac1* and *-2* and heterozygous for the *mig-2–like* (*mtl*)-null allele, *mtl[Δ]*, did not affect PEC AJs, SJs, or apical area (Fig. S3 G).

In individual and clusters of clones expressing DN Cdc42-N17, secondary and tertiary PECs exhibited increased apical area, whereas primary PECs had no change in apical area (Fig. S3 C). These phenotypes were clearly different from Cdc42 LOF clones,

which included decreases of all PEC apical areas (Fig. 2). In addition, expression of constitutively active Cdc42, Cdc42-V12, resulted in dramatic apical cell constriction (Fig. S3 E), which is in contrast to the increase in apical area seen when WT Cdc42 was overexpressed (Figs. 2 C and 3 C).

Cdc42 inhibits Rho1 activity at AJs

A key determinant of epithelial cell tension and contractility is the activity of the actomyosin cytoskeleton at AJs. Although Cdc42 activity does influence actin cytoskeletal dynamics, precisely how Cdc42 regulates actomyosin contractility at AJs is not clear. *Cdc42[4]* clonal cells had increased staining for F-actin and phospho-MLC (Ser19) at the level of AJs (Fig. 4, A and B; and Tables S3 and S4). Consistent with increased F-actin levels and myosin activity at AJs being associated with apical constriction, clones with LOF alleles of *twinstar* (*tsr*; *Drosophila cofilin*), which inhibits actin polymerization (Chen et al., 2001), and *slingshot* (*ssh*), which activates cofilin (Niwa et al., 2002), resulted in increased AJ-associated F-actin, as anticipated, and associated apical cell contraction (Fig. S2, B and C; and Tables S2 and S3). Similarly, expression of an active form of
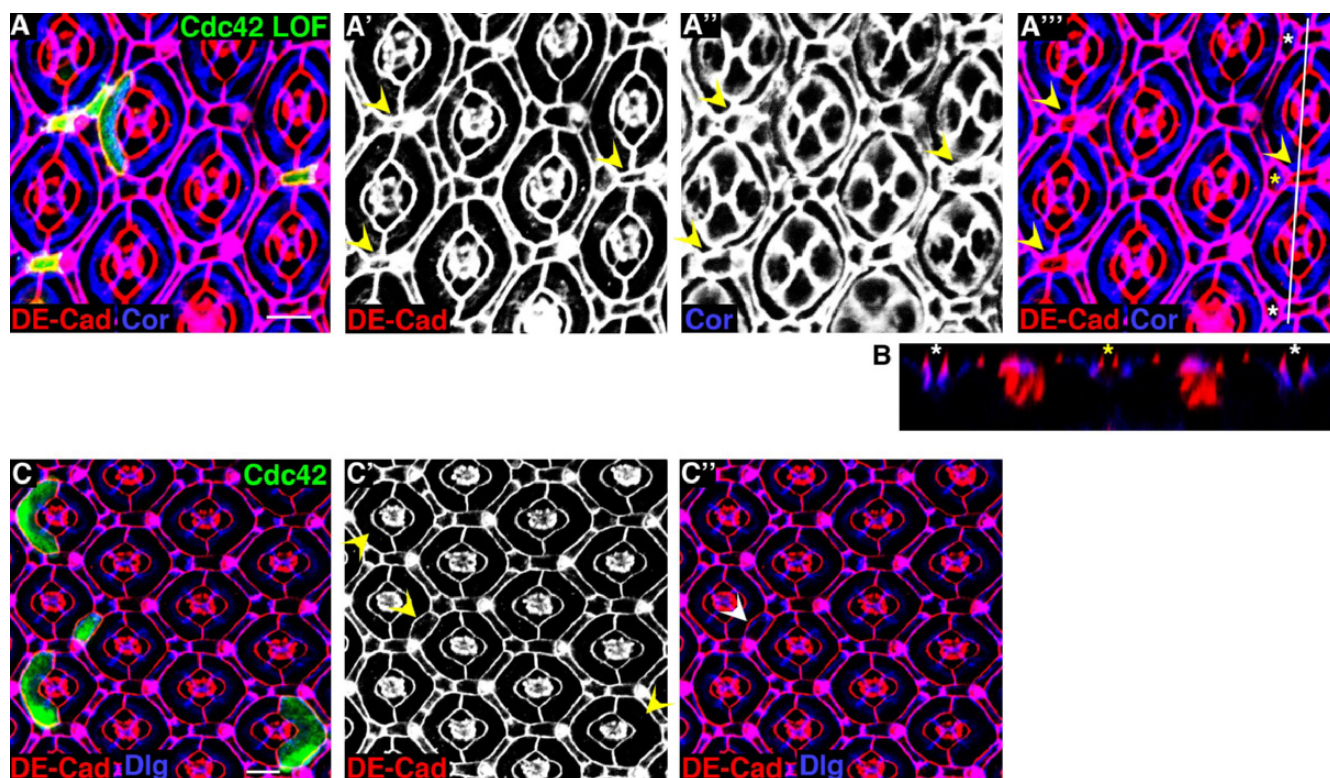
Figure 3. **Cdc42 specifically inhibits apical tension at AJs.** (A and B) Confocal immunofluorescent localization of DE-cadherin (DE-Cad; A, A′, A‴, and B) and Coracle (Cor; A and A″–B) in apical (A–A‴) and lateral (B) optical sections of *Cdc42⁴* MARCM clones. The white line (A‴) identifies where the lateral section (B) was taken. Yellow asterisks identify the *Cdc42⁴* MARCM clone, whereas white asterisks identify analogous nonclonal WT cells. Arrowheads identify AJs (A′ and A″) and SJs (A″ and A‴) around clonal cells. (C) Confocal immunofluorescent localization of DE-cadherin (C–C″) and Dlg (C and C″) in Flp-out clones overexpressing WT Cdc42. Arrowheads identify clonal cells. Bars, 10 µm.

Rho kinase (Rok–catalytic domain [CAT]; Verdier et al., 2006) resulted in increased phospho-MLC at AJs and apical constriction (Fig. S2 D and Tables S2 and S4). Collectively, one possibility these data suggested was that depletion of Cdc42 led to apical cell constriction through an increase in actomyosin tension at AJs.
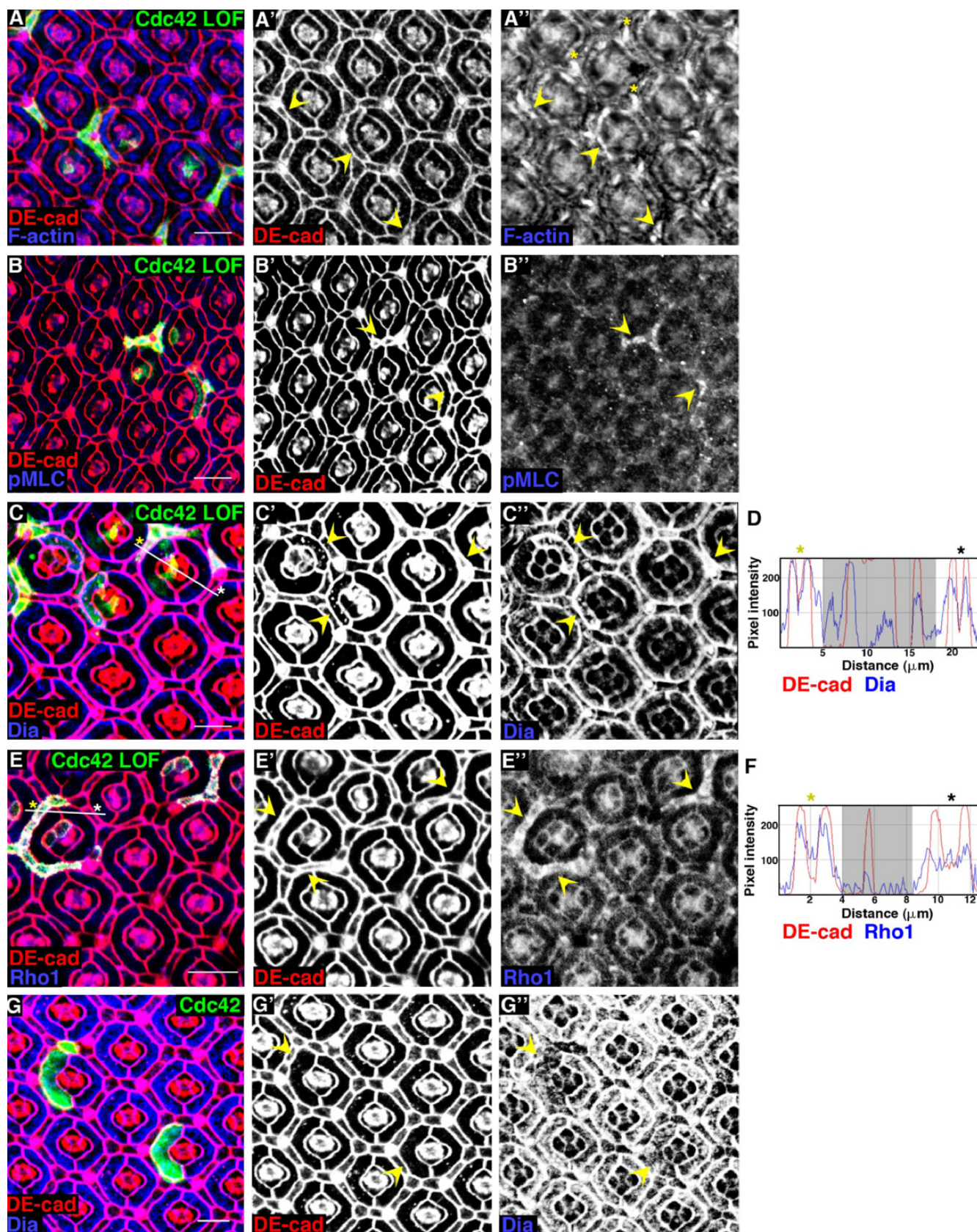
Rho promotes epithelial cell apical tension by increasing actomyosin activity (Conti and Adelstein, 2008), and *Rho1*-null clones exhibit increased apical cell area with decreased F-actin and phospho-MLC staining at AJs (Warner and Longmore, 2009). These opposing cellular phenotypes of Cdc42 and Rho1 LOF clones suggested the possibility that the increased apical cell tension apparent after Cdc42 depletion could result from increased Rho1 activity at the AJs caused by the absence of Cdc42.

To test this possibility, we first determined whether depletion of Cdc42 resulted in increased Rho1 activity. Activation of Rho correlates with its localization to AJs, where it can activate specific downstream effector proteins (Harder and Margolis, 2008). Thus, we determined the localization of Rho1 and the Rho1 effector Dia in *Cdc42⁴* clonal cells. Both Rho1 and Dia staining were increased at AJs in *Cdc42⁴* clonal cells (Fig. 4, C–F). In contrast, PEC clones overexpressing Cdc42 had decreased Rho1 and Dia at AJs (Fig. 4 G and Fig. S4 J). In a second approach, we used a GFP-tagged isoform of PKN (another Rho effector), PKNG58AeGFP, which associates with active Rho GTP as a surrogate marker for Rho1 activity (Simões et al., 2006). The l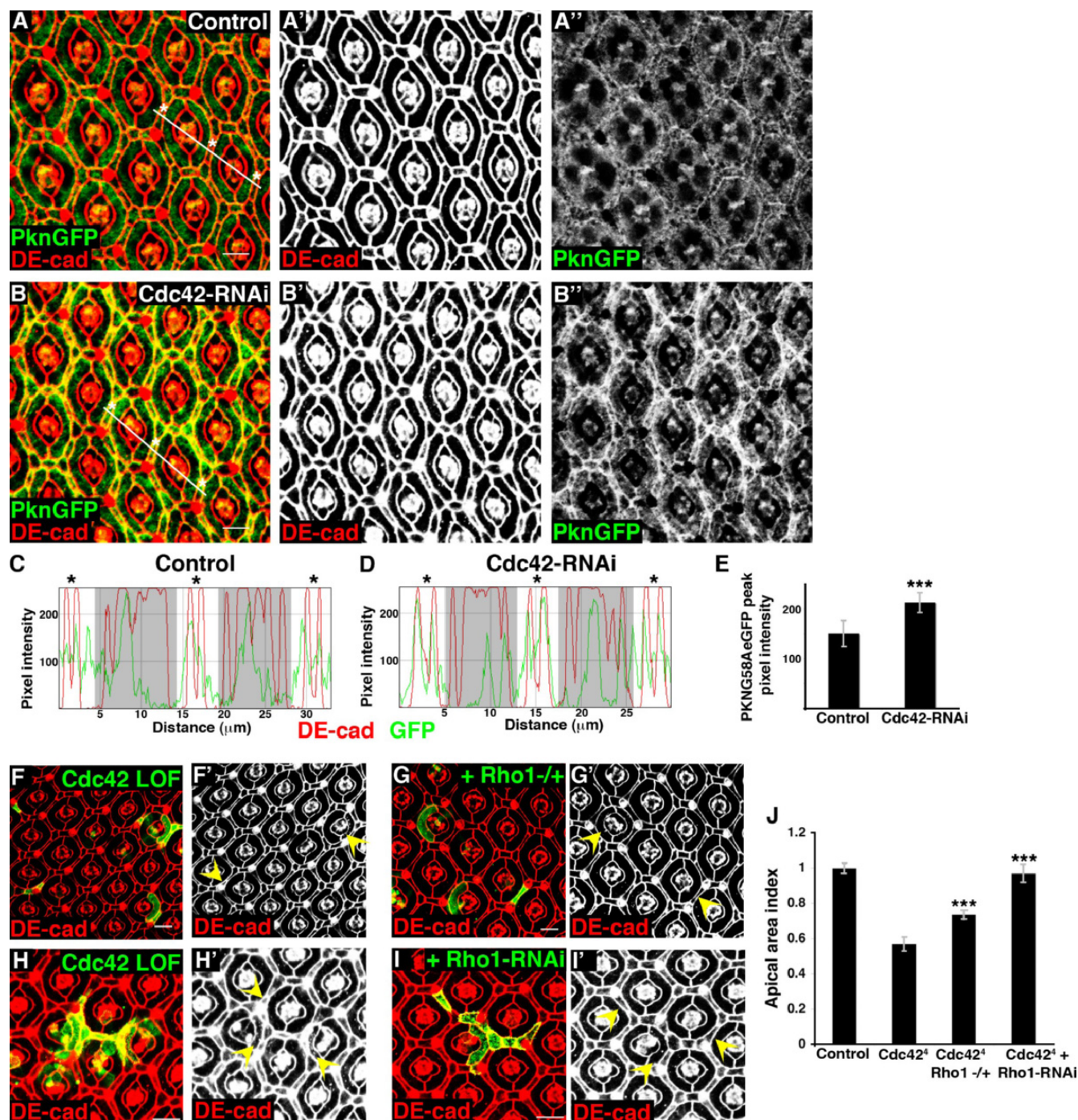evel of PKNG58AeGFP at AJs was increased in PECs depleted of Cdc42 (Fig. 5, A–E; and Table S5). Together, these data indicated that in epithelial cells depleted of Cdc42, Rho1 activity was increased at the level of AJs.

If Cdc42 controls apical cell tension through regulation of Rho1 activity, depletion of Rho1 in *Cdc42⁴* clonal cells would be predicted to rescue the decreased apical area seen in *Cdc42⁴* clonal cells. To test this, we expressed Rho1-RNAi in *Cdc42⁴* clones or removed a genomic copy of *Rho1* in the background of *Cdc42⁴* clones. By either approach, depletion of Rho1 in *Cdc42⁴* clonal cells rescued the decreased apical areas seen in *Cdc42⁴* clones alone (Fig. 5, F–J; and Table S2). As controls, heterozygous *Rho1* pupal eyes were indistinguishable from WT (unpublished data). Although depletion of Rho1 in Cdc42 LOF clones rescued the decreased apical area, SJs were still disrupted (Fig. S4 A). In addition, overexpression of Rho1 did not disrupt SJs despite causing apical constriction (Fig. S4 B), indicating that, in contrast to apical cell tension, Cdc42 regulated SJs independent of Rho1. Consistent with Cdc42 regulating apical cell tension through Rho1 (i.e., upstream), expression of Cdc42-RNAi, which alone caused decreased apical cell areas (Fig. 2 C and Fig. S2 A), had no effect on the increase in apical cell area in *Rho1*-null clones (Warner and Longmore, 2009). These genetic data, coupled with Rho1 activity profiles in Cdc42-depleted cells, indicated that Cdc42 depletion resulted in increased Rho1 activity at AJs, which increased actomyosin activity, apical cell tension, and thus, decreased apical cell area.

Figure 4. Cdc42 inhibits F-actin, phospho-MLC, Dia, and Rho1 localization at AJs. (A and B) Confocal immunofluorescent localization of DE-cadherin (DE-cad; A, A′, B, and B′), F-actin (A and A″), and phospho-MLC (pMLC; B and B″) in *Cdc42⁴* MARCM clones. Asterisks identify bristles around one ommatidium that have high levels of F-actin (A″). (C and E) Confocal immunofluorescent localization of DE-cadherin (C, C′, E, and E′), Dia (C and C″), and Rho1 (E and E″) in *Cdc42⁴* MARCM clones. (D) Pixel intensity profile of DE-cadherin and Dia immunofluorescence along the white line in C. Asterisks

Figure 5. **Cdc42 inhibits Rho1 activity at AJs to regulate apical cell tension.** (A) Confocal immunofluorescent localization of DE-cadherin (DE-cad; A and A′) in pupal eye expressing PKNG58AeGFP (PknGFP; A and A″) with *GMR-gal4*. (B) Confocal immunofluorescent localization of DE-cadherin (B and B′) in pupal eye expressing PKNG58AeGFP (B and B″) and Cdc42-RNAi with *GMR-gal4*. (C) Pixel intensity profile of DE-cadherin immunofluorescence and PKNG58AeGFP fluorescence in control PECs along the white line in A. Asterisks correspond to PECs in A. (D) Pixel intensity profile of DE-cadherin immunofluorescence and PKNG58AeGFP fluorescence in PECs expressing Cdc42-RNAi along the white line in B. Asterisks correspond to PECs in B. (C and D) Shaded regions cover cone cells and photoreceptors, which were not analyzed. (E) Quantification of PKNG58AeGFP peak pixel intensities at AJs in control or Cdc42-RNAi–expressing pupal eyes (see Table S5). Data are represented as mean ± SD. ***, P < 0.0001. (F and G) Confocal immuno-fluorescent localization of DE-cadherin in sibling pupal eyes with *Cdc42⁴* MARCM clones (F and F′) or *Cdc42⁴* MARCM clones in a *Rho1⁷²ᶠ* heterozygous background (G and G′). (H and I) Confocal immunofluorescent localization of DE-cadherin in sibling pupal eyes with *Cdc42⁴* MARCM clones (H and H′) or *Cdc42⁴* MARCM clones that express Rho1-RNAi (I and I′). (F–I) Arrowheads identify clonal cells. (J) Quantification of apical areas in clonal cells depleted of Cdc42 alone or with Rho1 also depleted (for apical area index, see Table S2). Data are represented as mean ± SD. ***, P < 0.001. Bars, 10 μm.

correspond to PECs in C. (F) Pixel intensity profile of DE-cadherin and Rho1 immunofluorescence along the white line in E. Asterisks correspond to PECs in E. (D and F) Shaded regions cover areas not analyzed. (G) Confocal immunofluorescent localization of DE-cadherin (G and G′) and Dia (G and G″) in Flp-out clones overexpressing WT Cdc42. (A–C, E, and G) Arrowheads identify clonal cells. Bars, 10 μm.
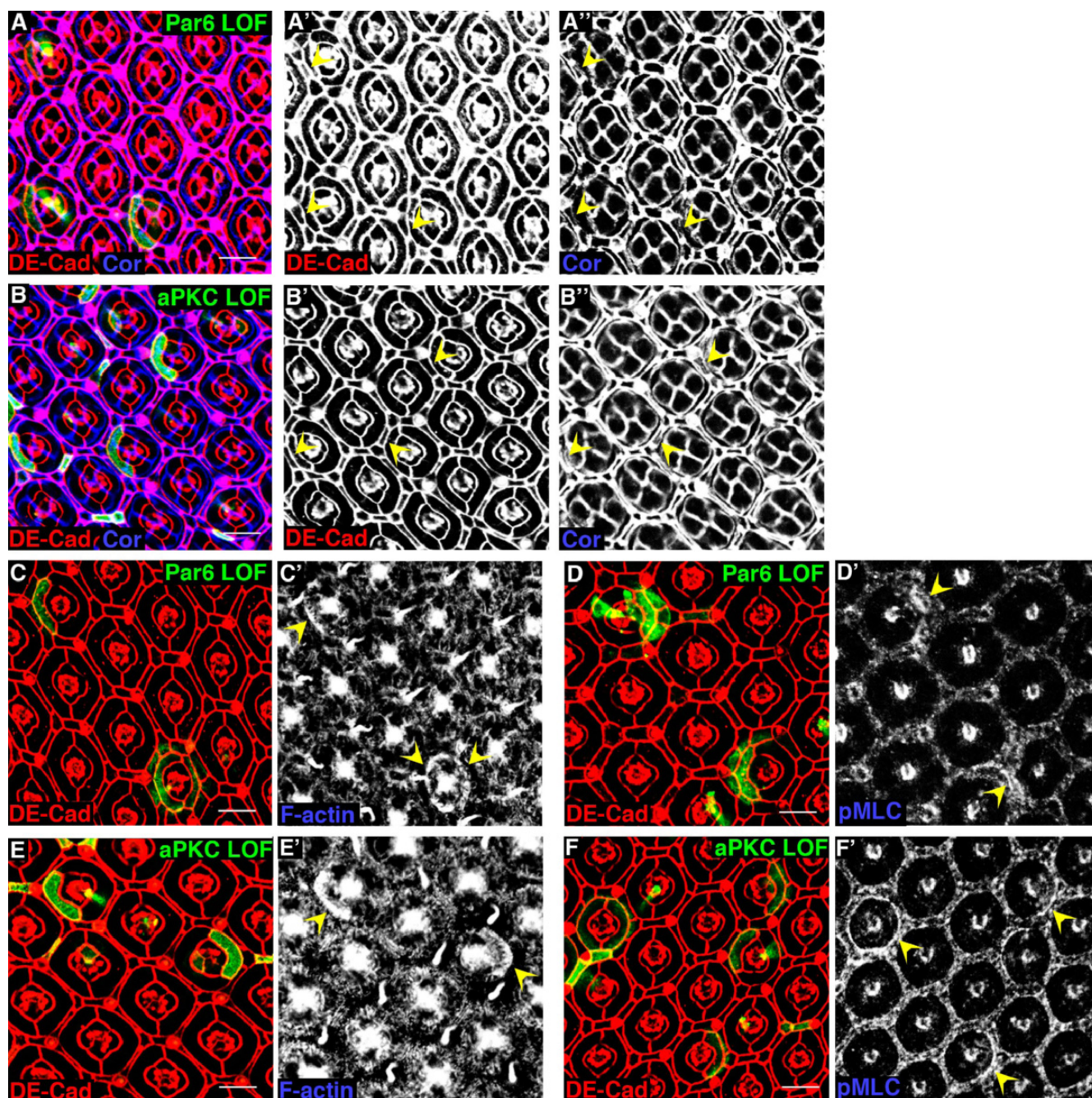
Figure 6. **Par6 and aPKC depletion phenocopies Cdc42 depletion.** (A and B) Confocal immunofluorescent localization of DE-cadherin (DE-Cad; A, A′, B, and B′) and Coracle (Cor; A, A″, B, and B″) in *par6^{Δ226}* MARCM clones (A–A″) and *aPKC^{k06403}* MARCM clones (B–B″). Arrowheads identify AJs (A′ and B′) and SJs (A″ and B″) around clonal primary PECs. (C–F) Confocal immunofluorescent localization of DE-cadherin (C, D, E, F), F-actin (C′ and E′), and phospho-MLC (pMLC; D′ and F′) in *par6^{Δ226}* (C–D′) and *aPKC^{k06403}* (E–F′) MARCM clones. Arrowheads identify clonal cells. Bars, 10 μm.

Par6–atypical PKC (aPKC) mediates Cdc42 functions in remodeling epithelium

Rho GTPases regulate cellular functions by interacting with and activating specific effector proteins, which mediate downstream cellular signaling events. Two major effectors downstream of Cdc42 are p21-activated kinase (Pak), which can phosphorylate and inactivate cofilin to promote actin polymerization, and Wiskott-Aldrich syndrome protein (Wsp), which promotes branched actin formation through activation of the

Arp2/3 complex (Heasman and Ridley, 2008). Surprisingly, unlike Cdc42 LOF clones, MARCM clones depleted of Pak, using the LOF allele *dPak^{16}*, or Wsp, using the LOF allele *wsp^3*, exhibited normal apical cell area and SJ organization (Fig. S4, C and D). This indicated that Cdc42 regulated apical cell tension and SJ organization independent of the effectors Pak and Wsp, at least individually.

Cdc42 is also present in a complex of highly conserved proteins that includes aPKC and Par3 and -6. To determine
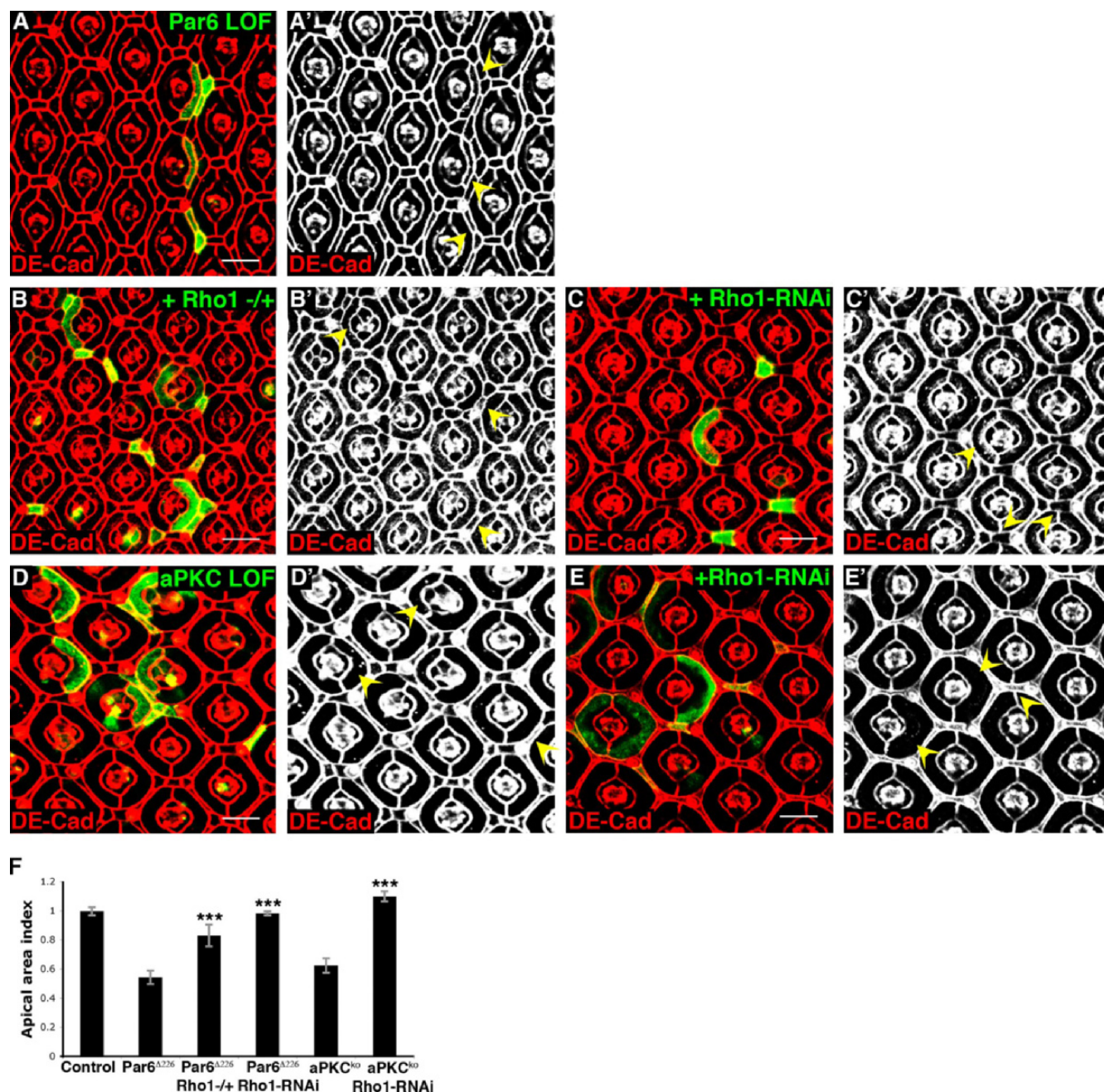
Figure 7. Par6 and aPKC inhibit apical tension in a Rho1-dependent manner. (A–C) Confocal immunofluorescent localization of DE-cadherin (DE-Cad) in *par6*^{Δ226} MARCM clones alone (A and A′), in a *Rho1*^{72F} heterozygous background (B and B′), or expressing Rho1-RNAi (C and C′). (D and E) Confocal immunofluorescent localization of DE-cadherin in *aPKC*^{k06403} MARCM clones alone (D and D′) or *aPKC*^{k06403} MARCM clones expressing Rho1-RNAi (E and E′). (A–E) Arrowheads identify clonal cells. (F) Quantification of apical areas in clonal cells depleted of Par6 or aPKC alone or with Rho1 also depleted (for apical area index, see Table S2). Data are represented as mean ± SD. ***, P ≤ 0.001. Bars, 10 µm.

whether members of this Par polarity complex (aPKC–Par3–Par6) mediated Cdc42 LOF phenotypes, we generated MARCM clones with LOF alleles of *Drosophila bazooka* (*baz*; *Drosophila Par3*), *aPKC*, and *par6*. Baz LOF clones did not affect apical area or SJ organization (Fig. S4 E). However, Par6 and aPKC LOF clones both phenocopied Cdc42 LOF clones, with decreased apical area and disrupted primary PEC SJs (Fig. 6, A and B; and Table S2). These data suggested that Cdc42 required its association with Par6–aPKC to regulate apical cell tension and maintain SJ organization.

To determine whether the decreased apical area in cells depleted of Par6 and aPKC also resulted from increased Rho1 activity, we depleted Rho1 in Par6 LOF or aPKC LOF clones. This rescued the decrease in apical area seen in Par6 or aPKC LOF clones (Fig. 7, A–F; and Table S2). In addition, Par6 and aPKC LOF clones had increased Rho1, F-actin, and phospho-MLC staining at AJs, which is consistent with increased Rho1 activation (Fig. 6, C–F; Fig. S4, K and L; and Tables S3 and S4). These data indicated that, like Cdc42 depletion, depletion of Par6 or aPKC increased Rho1 activity, which resulted in increased apical tension.
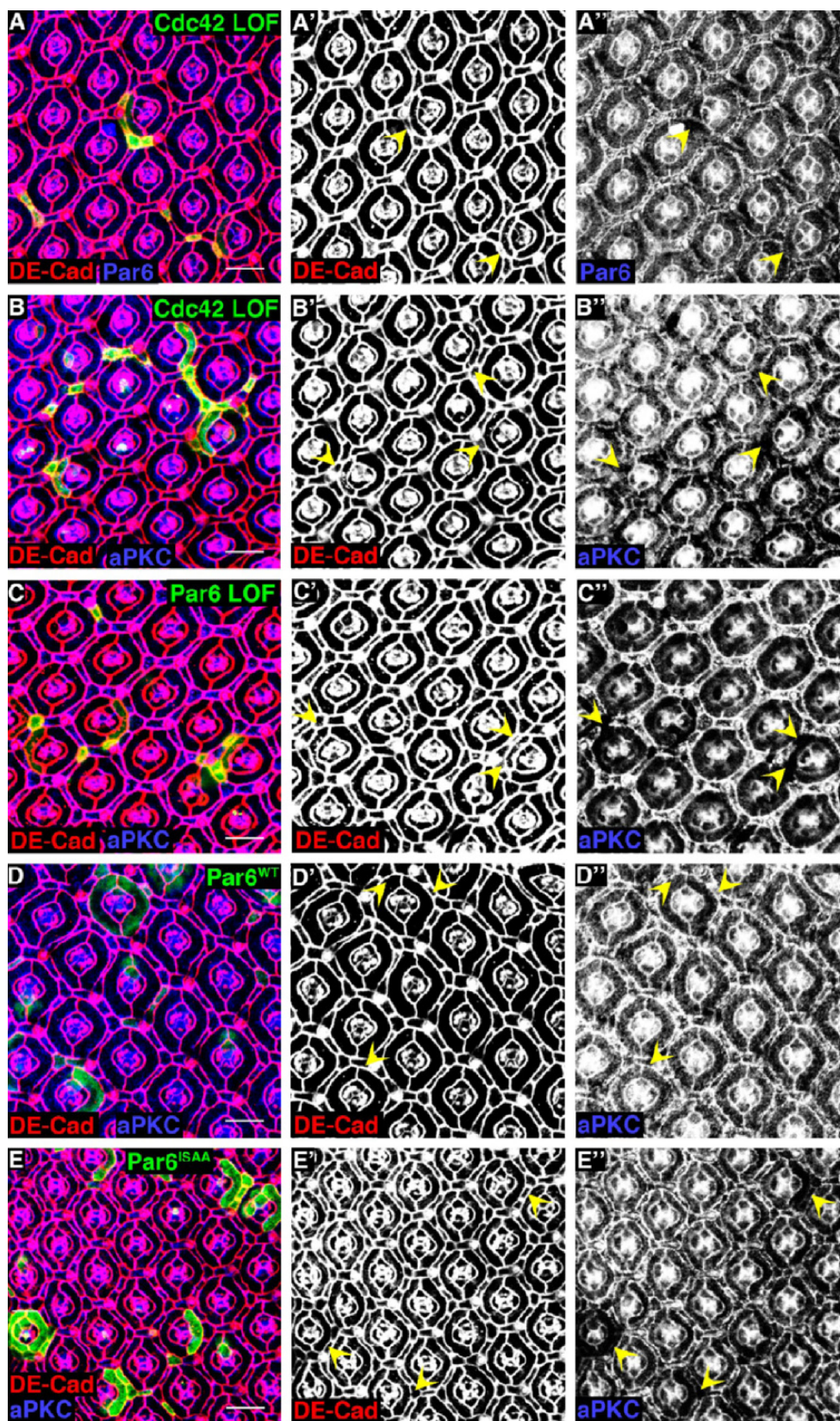
Figure 8. **Cdc42 localizes Par6 and aPKC to AJs.** (A and B) Confocal immunofluorescent localization of DE-cadherin (DE-Cad; A, A', B, and B'), Par6 (A and A"), and aPKC (B and B") in *Cdc42⁴* MARCM clones. Arrowheads identify AJs (A' and B'), Par6 (A"), and aPKC (B") between clonal cells. (C) Confocal immunofluorescent localization of DE-cadherin (C and C') and aPKC (C and C") in *par6^{Δ226}* MARCM clones. Arrowheads identify AJs (C') and aPKC (C") between clonal cells. (D and E) Confocal immunofluorescent localization of DE-cadherin (D, D', E, and E') and aPKC (D, D", E, and E") in Flp-out clones expressing either WT Par6 (Par6^{WT}; D–D") or Cdc42-binding mutant Par6 (Par6^{ISAA}; E–E"). Arrowheads identify AJs (D' and E') and aPKC (D" and E") between clonal cells. Bars, 10 μm.

Cdc42 inhibits Rho1 by localizing Par6–aPKC to the AJs

Cdc42 localizes Par6–aPKC to AJs through an interaction with Par6, which associates with and controls the activity of aPKC (Henrique and Schweisguth, 2003; Atwood et al., 2007). Consistent with this, both Par6 and aPKC were mislocalized from AJs between $Cdc42^4$ clonal cells (Fig. 8, A and B), and aPKC was mislocalized between $par6^{\Delta226}$ clonal cells (Fig. 8 C), as anticipated. Baz localization at AJs was not affected by Cdc42 depletion (Fig. S4 F). Therefore, we asked whether Par6's interaction with Cdc42 was critical for this complex to function in pupal eye PECs. Clones expressing the Cdc42-binding mutant Par6 phenocopied Cdc42, Par6, and aPKC LOF clones with decreased apical areas, mislocalized primary PEC SJ proteins (Fig. 9 B), and increased AJ-associated F-actin and phospho-MLC (not depicted). aPKC was also mislocalized from AJs between clonal cells expressing Cdc42-binding mutant Par6 (Fig. 8 E). As controls, clones expressing WT Par6 exhibited normal apical areas, SJ protein organization (Fig. 9 A), AJ-associated F-actin and phospho-MLC (not depicted), and aPKC localization (Fig. 8 D). In control experiments, the WT Par6 transgene was expressed at equal or higher levels than the Cdc42-binding mutant Par6 (Fig. S5, A–C).

In cells depleted of Cdc42, Par6, or aPKC or cells expressing a Cdc42-binding mutant Par6, apical area was decreased likely as a result of increased Rho1 activity. A common thread to all of these genetic manipulations was mislocalization or absence of aPKC from the AJs, suggesting that the increased Rho1 activity and resultant decreased apical areas in these cells could result from absence of aPKC activity at AJs. To test this possibility, we expressed either a membrane-associated, prenylated aPKC isoform, aPKC^{CAAX}, or WT aPKC, aPKC^{WT}, in Cdc42 LOF clones. aPKC^{WT} overexpression in $Cdc42^4$ clones did not rescue the decreased apical area; however, expression of aPKC^{CAAX} did (Fig. 9, C–F; and Table S2). In control experiments, in clones expressing aPKC^{WT} or aPKC^{CAAX} alone, apical area was not altered, aPKC^{WT} was expressed at equal or higher levels than aPKC^{CAAX}, and although aPKC^{WT} was diffusely localized within the cell, aPKC^{CAAX} localized to the membrane (Fig. S5, D and E).

Discussion

These data support a model in which Cdc42 limits epithelial cell apical tension by localizing Par6–aPKC to AJs, where aPKC inhibits Rho1 activity (Fig. 9 G). aPKC could do this either by directly modulating Rho1 activity or localization or more likely by either inhibiting a Rho guanine nucleotide exchange factor (GEF) or activating a Rho GTPase-activating protein (GAP), which would be predicted to be in the vicinity of the AJ. In this regard, a recent study identifying p190 Rho GAP as influencing RhoA activity downstream of Par6 to regulate dendritic spine morphogenesis in hippocampal neurons (Zhang and Macara, 2008) might implicate p190 Rho GAP as also regulating epithelial cell tension downstream of Cdc42. Alternatively, the E3 ubiquitin ligase Smurf, which has been shown to regulate RhoA degradation downstream of Cdc42–Par6–aPKC in mammalian

cells (Wang et al., 2003), functions in this regulation. In addition, as seen in other systems (Georgiou et al., 2008; Leibfried et al., 2008; Nakayama et al., 2008; Zhang and Macara, 2008), Par6–aPKC functions independently from Par3 in regulating epithelial cell tension.

Cdc42 depletion was recently demonstrated to decrease apical area of pupal notum epithelial cells (Georgiou et al., 2008; Leibfried et al., 2008), and it was suggested that this effect was caused by delamination of Cdc42-depleted cells as a result of increased DE-cadherin endocytosis, leading to decreased adhesion with neighboring cells. Although we also observed a role for Cdc42 in regulating DE-cadherin endocytosis in pupal eye PECs (Warner and Longmore, 2009), our data suggest that the decrease in PEC apical area is more likely caused by increased Rho1 activity at AJs as opposed to increased DE-cadherin endocytosis. In support of this, directly affecting DE-cadherin endocytosis by inhibiting Rab5 or -11 did not affect PEC apical area (Warner and Longmore, 2009). Also, overexpression of Cdc42 results in increased apical area, which would not be predicted if the apical area phenotype was caused by changes in DE-cadherin endocytosis.

Cdc42 can also influence actomyosin contractility through another effector, myotonic dystrophy kinase-related Cdc42-binding kinase (MRCK), which phosphorylates MLC and MLC phosphatase to effectively increase myosin activity. Indeed, Cdc42-MRCK was found to positively cooperate with Rho-ROCK signaling in tumor cell line invasion in ex vivo cultures (Wilkinson et al., 2005). In contrast, in the remodeling pupal eye epithelium, we found that Cdc42 inhibits actomyosin activity by antagonizing Rho activity in vivo. The effect of Cdc42-MRCK on carcinoma cell line contractility was cell type dependent, with some cell types (e.g., A375m2 cells) more dependent on Rho-ROCK than Cdc42-MRCK for maintaining myosin activity. Therefore, Cdc42 may have different effects on actomyosin contractility in different epithelial cells. Alternatively, although this study analyzed individual tumor cell lines spread on tissue culture plastic, the regulation of epithelial cell contractility in a polarized epithelial monolayer in vivo analyzed in this study is likely to be distinct.

We also demonstrated that Cdc42 depletion in PECs specifically disrupted SJs but not AJs and only around primary PECs. Several differences exist between primary PECs and secondary and tertiary PECs (Bao and Cagan, 2005; Nagaraj and Banerjee, 2007), and these differences may affect the sensitivity of SJs to Cdc42 depletion. How Cdc42–Par6–aPKC maintains primary PEC SJs is still an unanswered question; perhaps this involves the complex's role in endocytosis. Studies in *Drosophila* notum reported effects on AJs but not SJs after Cdc42 depletion (Georgiou et al., 2008; Leibfried et al., 2008). However, one important difference between the pupal notum and the pupal eye is the proliferation state, with the notum epithelium undergoing proliferation and the pupal eye PECs being postmitotic. Perhaps the proliferation state of epithelial cells dictates the junctional phenotypes resulting from Cdc42 depletion. For instance, proliferating epithelial cells are forming new intercellular junctions, whereas postmitotic nonproliferating epithelial cells mostly remodel existing junctions.
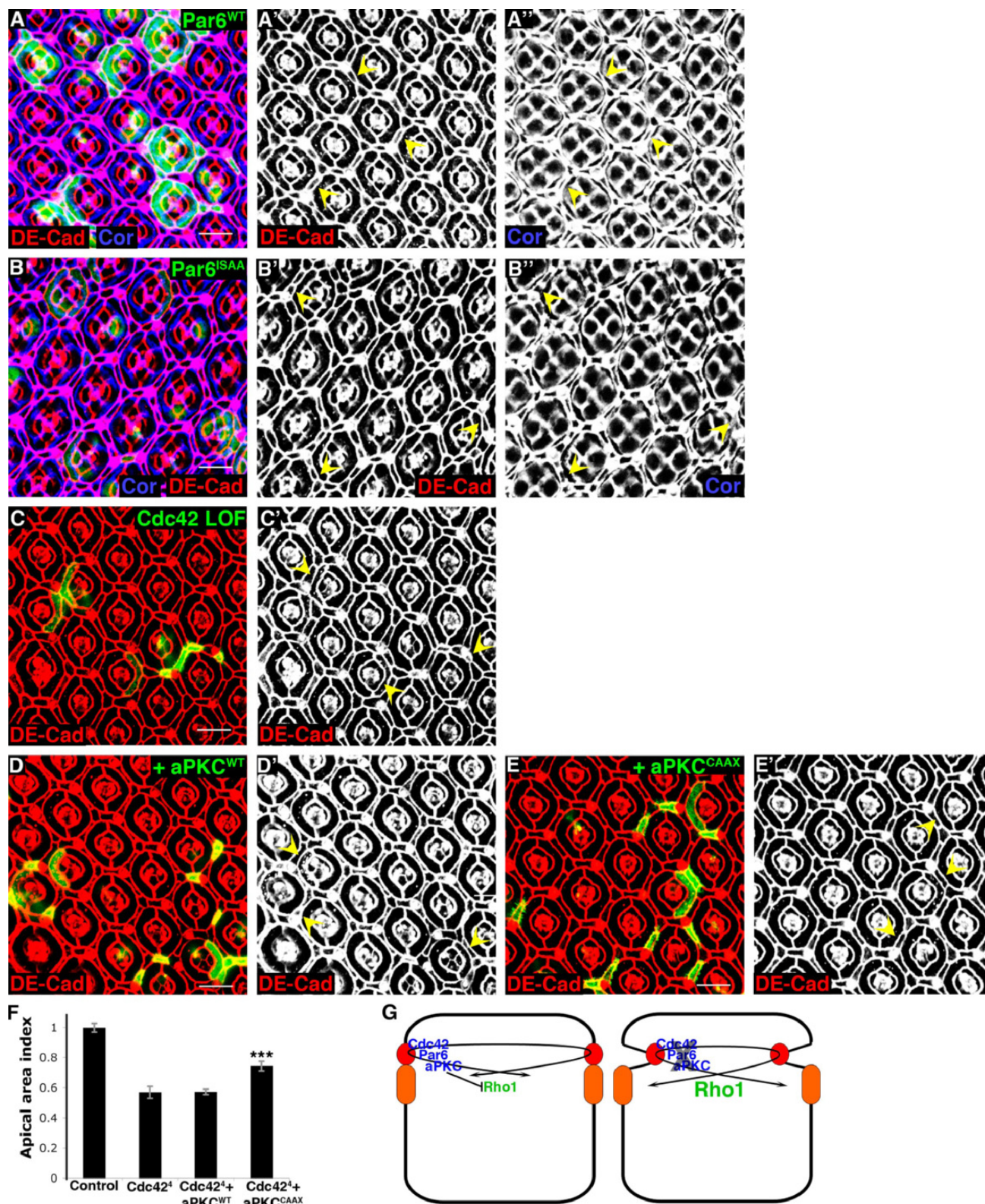
Figure 9. **Cdc42 inhibits Rho1 activity by localizing Par6–aPKC to AJs.** (A and B) Confocal immunofluorescent localization of DE-cadherin (DE-Cad; A, A', B, and B') and Coracle (Cor; A, A'', B, and B'') in Flp-out clones expressing WT Par6 (Par6^{WT}; A–A'') or Cdc42-binding mutant Par6 (Par6^{ISAA}; B–B''). Arrowheads identify AJs (A' and B') and SJs (A'' and B'') around clonal primary PECs. (C–E) Confocal immunofluorescent localization of DE-cadherin in *Cdc42^4* MARCM clones alone (C and C'), expressing WT aPKC (aPKC^{WT}; D and D'), or expressing membrane-associated aPKC^{CAAX} (E and E'). Arrowheads identify clonal cells. (F) Quantification of apical areas in clonal cells depleted of Cdc42 alone, expressing aPKC^{WT}, or expressing aPKC^{CAAX} (for apical area index, see Table S2). Data are represented as mean ± SD. ***, P < 0.001. (G) Model for Cdc42 function in PECs. Cdc42–Par6 localizes aPKC to AJs, where aPKC inhibits Rho1 activity and its associated actomyosin tension. When Cdc42–Par6–aPKC localization to AJs is disrupted, Rho1 activation and actomyosin tension at AJs increases. Bars, 10 μm.

An important technical consideration resulting from our study was that we observed opposite effects on epithelial junctions and apical tension depending on whether Cdc42 was genetically depleted or inhibited by expressing dominant-inhibitory isoforms of Cdc42. Rac-DN expression also disrupted AJs (Fig. S3 F; Bruinsma et al., 2007), whereas clones genetically depleted of Rac1 and -2 and Mtl did not (Fig. S3 G). DN Rho proteins, in general, are thought to function by binding and inhibiting Rho GEFs. Cdc42 and Rac often share upstream GEFs, and Cdc42- and Rac-DN expression in the pupal eye both disrupted AJs but not SJs. Therefore, one possible explanation for differences between phenotypes resulting from genetic depletion of Cdc42 or Rac compared with inhibition of activation by Cdc42- or Rac-DN expression was that these DN proteins inhibit GEFs common to Cdc42 and Rac, thereby inhibiting both Cdc42 and Rac activities. However, even pupal eyes depleted of Rac1 and -2 and Mtl and Cdc42 had completely intact AJs (Fig. S3 H). Perhaps Cdc42- and Rac-DN expression disrupts AJs by binding GEFs that normally activate Rho1, which, when genetically depleted, does result in disrupted AJs (Warner and Longmore, 2009). Although we observed many differences between Cdc42-DN expression and Cdc42 LOF analysis, a recent study in *Drosophila* embryonic ventral neuroectoderm reported AJ disruptions associated with both Cdc42-DN expression and Cdc42 LOF (Harris and Tepass, 2008). Regardless, these data emphasize that caution is needed when interpreting results using Rho GTPase dominant mutant proteins, particularly in vivo, and results should be corroborated with genetic LOF data at all stages of analysis.

Our results showing that the Cdc42–Par6–aPKC polarity complex negatively regulates Rho1 activity draws parallels to events that occur during epithelial tumor (carcinoma) development and progression. Loss of apical–basal polarity, as a result of mislocalization of Cdc42–Par6–aPKC in proliferating epithelial cells, is considered an early and critical event for carcinoma development (Aranda et al., 2008). In addition, activation of RhoA is often associated with increased cancer cell invasion, migration, and metastasis (Heasman and Ridley, 2008). Thus, in addition to its role in the establishment of apical–basal polarity in forming epithelia, the Cdc42–Par6–aPKC polarity complex may also be required to limit Rho activity at AJs and thus modulate apical tension so as to shape the final epithelium.

Materials and methods

Drosophila stocks
All crosses and staging were performed at 25°C unless otherwise noted. *w^1118* was used as WT. Stocks are described in FlyBase (http://flybase .bio.indiana.edu). *Glass multimer reporter* (*GMR*)–*gal4, tubulin-gal80^ts, Cdc42^4* FRT19A, *Cdc42^2* FRT19A, upstream activating sequence (UAS)– GFP, *pak^16* FRT82B, UAS–Cdc42-N17, UAS–Rac-N17, UAS–Cdc42-V12, *Rho1^72F, ssh^1–11* FRT82B, and *rac1^J11rac2^Δ* FRT2A *mtl^Δ* were provided by the Bloomington Drosophila Stock Center; *patched-gal4, wsp^3* FRT82B, and *scrib^1* FRT82B were provided by R. Cagan (Mount Sinai Medical Center, New York, NY); UAS-PKNG58AeGFP was provided by A. Jacinto (Instituto Gulbenkian de Ciência, Oeiras, Portugal); *tsr^99E* FRT42D was provided by F. Pichaud (University College London, London, England UK); UAS–Rok-CAT was provided by G.-C. Chen (Academia Sinica, Taipei, Taiwan); *par6^Δ226* FRT19A, *apkc^k06403* FRTG13, *baz^4* FRT19A, UAS-aPKC^WT, UAS-aPKC^CAAX, and *dlg^m52* were provided by C. Doe (University of Oregon,

Eugene, OR); and UAS–Dlg-RNAi was provided by the Vienna Drosophila RNAi Center. Rho1- and Cdc42-RNAi were generated using fragments of *Rho1* and *Cdc42* amplified from Canton-S cDNA to target 325–786 bp after the start codon of *Rho1* and 191 bp before to 278 bp after the start codon of *Cdc42*, respectively, as was previously described (Warner and Longmore, 2009).

Clonal analysis and genetics
To generate Flp-out clones overexpressing a transgene, progeny from Act5C>y^+>gal4, UAS-GFP; heat shock Flp (hsFLP) crossed to the following genotypes were heat-shocked for 30 min at 37°C as third instar larvae or early pupae: (a) UAS–Cdc42-RNAi, (b) UAS-Cdc42, (c) UAS-aPKC^WT, (d) UAS-aPKC^CAAX, (e) UAS–Cdc42-N17, (f) UAS–Rok-CAT, (g) UAS-Par6^WT, and (h) UAS-Par6^ISAA. Clones were marked by the presence of GFP.

MARCM clones were generated by heat shocking larvae with the following genotypes for 1 h at 37°C: (a) *Cdc42^2*, FRT19A/hsFLP, *tub-gal80*, FRT19A; UAS-GFP, UAS-*lacZ*/+; *tub-gal4*/+, (b) *Cdc42^4*, FRT19A/hsFLP, *tub-gal80*, FRT19A; UAS-GFP, UAS-*lacZ*/+; *tub-gal4*/+, (c) *baz^4*, FRT19A/hsFLP, *tub-gal80*, FRT19A; UAS-GFP, UAS-*lacZ*/+; *tub-gal4*/+, (d) *par6^Δ226*, FRT19A/hsFLP, *tub-gal80*, FRT19A; UAS-GFP, UAS-*lacZ*/+; *tub-gal4*/+, (e) hsFLP, UAS-GFP; *tsr^99E*, FRT42D/*tub-gal80*, FRT42D; *tub-gal4*/+, (f) hsFLP, UAS-GFP; *tub-gal4*/+; *pak^16*, FRT82D/*tub-gal80*, FRT82D, (g) hsFLP, UAS-GFP; *tub-gal4*/+; *wsp^3*, FRT82D/*tub-gal80*, FRT82D, (h) hsFLP, UAS-GFP; *tub-gal4*/+; *ssh^1–11*, FRT82D/*tub-gal80*, FRT82D, (i) hsFLP, UAS-GFP; *aPKC^k06403*, FRTG13/*tub-gal80*, FRTG13; *tub-gal4*/+, (j) hsFLP, UAS-GFP; *GMR-gal4*/+; *rac1^J11*, *rac2^Δ*, FRT2A, *mtl^Δ*/*tub-gal80*, FRT2A, (k) *Cdc42^4*, FRT19A/hsFLP, *tub-gal80*, FRT19A; UAS-GFP, UAS-*lacZ*/UAS–Rho1-RNAi; *tub-gal4*/+, (l) *Cdc42^4*, FRT19A/hsFLP, *tub-gal80*, FRT19A; UAS-GFP, UAS-*lacZ*/UAS-Cdc42; *tub-gal4*/+, (m) *Cdc42^4*, FRT19A/hsFLP, *tub-gal80*, FRT19A; UAS-GFP, UAS-*lacZ*/Rho1^72F; *tub-gal4*/+, (n) *Cdc42^4*, FRT19A/hsFLP, *tub-gal80*, FRT19A; UAS-GFP, UAS-*lacZ*/UAS-aPKC^WT; *tub-gal4*/+, (o) *Cdc42^4*, FRT19A/hsFLP, *tub-gal80*, FRT19A; UAS-GFP, UAS-*lacZ*/UAS-aPKC^CAAX; *tub-gal4*/+, (p) *par6^Δ226*, FRT19A/hsFLP, *tub-gal80*, FRT19A; UAS-GFP, UAS-*lacZ*/+; *tub-gal4*/UAS-Par6^WT, (q) *par6^Δ226*, FRT19A/hsFLP, *tub-gal80*, FRT19A; UAS-GFP, UAS-*lacZ*/+; *tub-gal4*/UAS-Par6^ISAA, (r) *par6^Δ226*, FRT19A/hsFLP, *tub-gal80*, FRT19A; UAS-GFP, UAS-*lacZ*/UAS–Rho1-RNAi; *tub-gal4*/+, (s) *par6^Δ226*, FRT19A/ hsFLP, *tub-gal80*, FRT19A; UAS-GFP, UAS-*lacZ*/Rho1^72F; *tub-gal4*/+, and (t) hsFLP, UAS-GFP; *aPKC^k06403*, FRTG13/*tub-gal80*, FRTG13; *tub-gal4*/ UAS–Rho1-RNAi. Clones were marked by the presence of GFP.

Expression of either GFP alone or GFP and Cdc42-RNAi with *patched-gal4* in the pupal wing was performed by crossing *patched-gal4*, UAS-GFP, *tub-gal80^ts*/SM6a-TM6b to *w^1118* or UAS–Cdc42-RNAi/SM6a-TM6b at 18°C. Progeny were shifted to 29°C 3–4 d after egg laying and dissected at 18 h APF.

Immunofluorescence
Pupal eyes or wings were dissected in PBS, fixed in 4% paraformaldehyde for 45 min, washed once in PBS-T (PBS/0.1% Triton X-100), washed twice in PAXD (PBS containing 1% BSA, 0.3% Triton X-100, and 0.3% deoxycholate), and washed once in PAXDG (PAXD with 5% goat serum), all on ice. The tissue was then incubated overnight at 4°C with primary antibodies diluted in PAXDG, washed three times in PBS-T, and incubated overnight at 4°C with secondary antibodies diluted in PAXDG. After washing twice in PBS-T, the tissue was postfixed in 4% paraformaldehyde for 25 min at room temperature, washed twice in PBS-T, and mounted in Vectashield mounting media (Vector Laboratories). Antibodies used were rat anti–DE-cadherin (1:20), mouse anti-Armadillo (1:500), mouse anti-Dlg (1:50), mouse anti-Rho1 (1:20), mouse anti-Coracle (1:20; all from the Developmental Studies Hybridoma Bank), rabbit anti-Dia (1:500; from S. Wasserman, University of California San Diego, La Jolla, CA), rat anti-Crbs (1:500; from U. Tepass, University of Toronto, Toronto, Ontario, Canada), rabbit anti-Baz (1:500; from A. Wodarz, Georg-August-Universität Göttingen, Göttingen, Germany), guinea pig anti-Scrib (1:500; from D. Bilder, University of California, Berkeley, Berkeley, CA), rabbit anti-Par6 (1:500; from J. Knoblich, Institute of Molecular Biotechnology, Vienna, Austria), rabbit anti-aPKC (C-20; 1:200; Santa Cruz Biotechnology, Inc.), and rabbit anti–phospho-MLC 2 (Ser19; 1:20; Cell Signaling Technology). Rhodamine-phalloidin (1:500; Invitrogen) was added in the primary and secondary antibody incubations to visualize F-actin. Secondary antibodies used were Alexa Fluor 488 and 568 (Invitrogen) and Cy5 (Jackson ImmunoResearch Laboratories, Inc.). Immunofluorescence was analyzed on a confocal microscope (LSM 510; Carl Zeiss, Inc.) using a Plan-Apochromat 63× NA 1.4 oil objective (Carl Zeiss, Inc.) at room temperature with LSM 510 software (Carl Zeiss, Inc.). Photoshop (Adobe) was used to minimally adjust brightness and contrast to whole images.

Quantification and statistics

Images were analyzed using ImageJ version 1.38 (National Institutes of Health). Apical area indices were calculated as the ratio of a clonal cell apical area divided by an analogous, neighboring nonclonal cell apical area at AJs. F-actin indices were calculated as the ratio of phalloidin staining pixel intensity in a clonal cell divided by that in an analogous, neighboring nonclonal cell. Phospho-MLC indices were calculated as the ratio of phospho-MLC immunofluorescence pixel intensity in a clonal cell divided by that in an analogous, neighboring nonclonal cell. Pixel intensities for phalloidin staining and phospho-MLC immunofluorescence at AJs were determined by outlining DE-cadherin around a single cell in a confocal image and measuring the mean pixel value within that area. PKNG58AeGFP peak pixel intensities were determined from plotting and listing pixel values across a line drawn through PEC AJs (as shown in Fig. 5, A and B). P-values were calculated using unpaired, two-sided Student's t tests.

Online supplemental material

Fig. S1 shows DE-cadherin localization in Dlg and Scrib LOF clones. Fig. S2 shows decreased apical areas in clones expressing Cdc42-RNAi, increased F-actin in Tsr and Ssh LOF clones, and increased phospho-MLC levels in clones expressing Rok-CAT. Fig. S3 shows nonspecific phenotypes from the expression of Cdc42 and Rac dominant proteins. Fig. S4 shows SJs in clones overexpressing Rho1, Pak, Wsp, and Baz LOF clones, Baz and Crbs localization in Cdc42 LOF clones, and Rho1 localization in clones overexpressing Cdc42 and in Par6 and aPKC LOF clones. Fig. S5 shows Par6 localization in clones expressing Par6[WT] and Par6[ISAA], aPKC localization in clones expressing aPKC[WT] and aPKC[CAAX], and Cdc42-RNAi expression in the pupal wing. Table S1 quantifies SJ mislocalization in Cdc42 LOF clones and Cdc42 LOF clones expressing Cdc42. Table S2 quantifies apical areas of Cdc42, Par6, aPKC, Tsr, and Ssh LOF clones and Cdc42-overexpressing and Rok-CAT–expressing clones. Table S3 quantifies F-actin at AJs in Cdc42, Par6, aPKC, Tsr, and Ssh LOF clones. Table S4 quantifies phospho-MLC at AJs in Cdc42, Par6, and aPKC LOF clones and Rok-CAT–expressing clones. Table S5 quantifies PKNG58AeGFP peak pixel intensity at AJs in control and Cdc42-RNAi–expressing PECs. Online supplemental material is available at http://www.jcb.org/cgi/content/full/jcb.200906047/DC1.

References

Aranda, V., M.E. Nolan, and S.K. Muthuswamy. 2008. Par complex in cancer: a regulator of normal cell polarity joins the dark side. *Oncogene.* 27:6878–6887. doi:10.1038/onc.2008.340

Atwood, S.X., C. Chabu, R.R. Penkert, C.Q. Doe, and K.E. Prehoda. 2007. Cdc42 acts downstream of Bazooka to regulate neuroblast polarity through Par-6 aPKC. *J. Cell Sci.* 120:3200–3206. doi:10.1242/jcs.014902

Bao, S., and R. Cagan. 2005. Preferential adhesion mediated by Hibris and Roughest regulates morphogenesis and patterning in the *Drosophila* eye. *Dev. Cell.* 8:925–935. doi:10.1016/j.devcel.2005.03.011

Bilder, D. 2004. Epithelial polarity and proliferation control: links from the *Drosophila* neoplastic tumor suppressors. *Genes Dev.* 18:1909–1925. doi:10.1101/gad.1211604

Bruinsma, S.P., R.L. Cagan, and T.J. Baranski. 2007. Chimaerin and Rac regulate cell number, adherens junctions, and ERK MAP kinase signaling in the *Drosophila* eye. *Proc. Natl. Acad. Sci. USA.* 104:7098–7103. doi:10.1073/pnas.0701686104

Burridge, K., and K. Wennerberg. 2004. Rho and Rac take center stage. *Cell.* 116:167–179. doi:10.1016/S0092-8674(04)00003-0

Cagan, R.L., and D.F. Ready. 1989. The emergence of order in the *Drosophila* pupal retina. *Dev. Biol.* 136:346–362. doi:10.1016/0012-1606(89)90261-3

Chen, J., D. Godt, K. Gunsalus, I. Kiss, M. Goldberg, and F.A. Laski. 2001. Cofilin/ADF is required for cell motility during *Drosophila* ovary development and oogenesis. *Nat. Cell Biol.* 3:204–209. doi:10.1038/35055120

Conti, M.A., and R.S. Adelstein. 2008. Nonmuscle myosin II moves in new directions. *J. Cell Sci.* 121:11–18. doi:10.1242/jcs.007112

Furuse, M., and S. Tsukita. 2006. Claudins in occluding junctions of humans and flies. *Trends Cell Biol.* 16:181–188. doi:10.1016/j.tcb.2006.02.006

Georgiou, M., E. Marinari, J. Burden, and B. Baum. 2008. Cdc42, Par6, and aPKC regulate Arp2/3-mediated endocytosis to control local adherens junction stability. *Curr. Biol.* 18:1631–1638. doi:10.1016/j.cub.2008.09.029

Harder, J.L., and B. Margolis. 2008. SnapShot: tight and adherens junction signaling. *Cell.* 133:1118–1118.e2. doi:10.1016/j.cell.2008.06.002

Harris, K.P., and U. Tepass. 2008. Cdc42 and Par proteins stabilize dynamic adherens junctions in the *Drosophila* neuroectoderm through regulation of apical endocytosis. *J. Cell Biol.* 183:1129–1143. doi:10.1083/jcb.200807020

Hayashi, T., and R.W. Carthew. 2004. Surface mechanics mediate pattern formation in the developing retina. *Nature.* 431:647–652. doi:10.1038/nature02952

Heasman, S.J., and A.J. Ridley. 2008. Mammalian Rho GTPases: new insights into their functions from in vivo studies. *Nat. Rev. Mol. Cell Biol.* 9:690–701. doi:10.1038/nrm2476

Henrique, D., and F. Schweisguth. 2003. Cell polarity: the ups and downs of the Par6/aPKC complex. *Curr. Opin. Genet. Dev.* 13:341–350. doi:10.1016/S0959-437X(03)00077-7

Homem, C.C., and M. Peifer. 2008. Diaphanous regulates myosin and adherens junctions to control cell contractility and protrusive behavior during morphogenesis. *Development.* 135:1005–1018. doi:10.1242/dev.016337

Hutterer, A., J. Betschinger, M. Petronczki, and J.A. Knoblich. 2004. Sequential roles of Cdc42, Par-6, aPKC, and Lgl in the establishment of epithelial polarity during *Drosophila* embryogenesis. *Dev. Cell.* 6:845–854. doi:10.1016/j.devcel.2004.05.003

Ito, K., W. Awano, K. Suzuki, Y. Hiromi, and D. Yamamoto. 1997. The *Drosophila* mushroom body is a quadruple structure of clonal units each of which contains a virtually identical set of neurones and glial cells. *Development.* 124:761–771.

Kobielak, A., H.A. Pasolli, and E. Fuchs. 2004. Mammalian formin-1 participates in adherens junctions and polymerization of linear actin cables. *Nat. Cell Biol.* 6:21–30. doi:10.1038/ncb1075

Lee, T., and L. Luo. 1999. Mosaic analysis with a repressible cell marker for studies of gene function in neuronal morphogenesis. *Neuron.* 22:451–461. doi:10.1016/S0896-6273(00)80701-1

Leibfried, A., R. Fricke, M.J. Morgan, S. Bogdan, and Y. Bellaiche. 2008. *Drosophila* Cip4 and WASp define a branch of the Cdc42-Par6-aPKC pathway regulating E-cadherin endocytosis. *Curr. Biol.* 18:1639–1648. doi:10.1016/j.cub.2008.09.063

Martin-Belmonte, F., A. Gassama, A. Datta, W. Yu, U. Rescher, V. Gerke, and K. Mostov. 2007. PTEN-mediated apical segregation of phosphoinositides controls epithelial morphogenesis through Cdc42. *Cell.* 128:383–397. doi:10.1016/j.cell.2006.11.051

Montell, D.J. 2008. Morphogenetic cell movements: diversity from modular mechanical properties. *Science.* 322:1502–1505. doi:10.1126/science.1164073

Nagaraj, R., and U. Banerjee. 2007. Combinatorial signaling in the specification of primary pigment cells in the *Drosophila* eye. *Development.* 134:825–831. doi:10.1242/dev.02788

Nakayama, M., T.M. Goto, M. Sugimoto, T. Nishimura, T. Shinagawa, S. Ohno, M. Amano, and K. Kaibuchi. 2008. Rho-kinase phosphorylates PAR-3 and disrupts PAR complex formation. *Dev. Cell.* 14:205–215. doi:10.1016/j.devcel.2007.11.021

Niwa, R., K. Nagata-Ohashi, M. Takeichi, K. Mizuno, and T. Uemura. 2002. Control of actin reorganization by Slingshot, a family of phosphatases that dephosphorylate ADF/cofilin. *Cell.* 108:233–246. doi:10.1016/S0092-8674(01)00638-9

Olson, M.F., and E. Sahai. 2009. The actin cytoskeleton in cancer cell motility. *Clin. Exp. Metastasis.* 26:273–287. doi:10.1007/s10585-008-9174-2

Sahai, E., and C.J. Marshall. 2002. ROCK and Dia have opposing effects on adherens junctions downstream of Rho. *Nat. Cell Biol.* 4:408–415. doi:10.1038/ncb796

Schwamborn, J.C., and A.W. Püschel. 2004. The sequential activity of the GTPases Rap1B and Cdc42 determines neuronal polarity. *Nat. Neurosci.* 7:923–929. doi:10.1038/nn1295

Simões, S., B. Denholm, D. Azevedo, S. Sotillos, P. Martin, H. Skaer, J.C. Hombría, and A. Jacinto. 2006. Compartmentalisation of Rho regulators directs cell invagination during tissue morphogenesis. *Development.* 133:4257–4267. doi:10.1242/dev.02588

Verdier, V., Guang-Chao-Chen, and J. Settleman. 2006. Rho-kinase regulates tissue morphogenesis via non-muscle myosin and LIM-kinase during *Drosophila* development. *BMC Dev. Biol.* 6:38. doi:10.1186/1471-213X-6-38

Wang, H.R., Y. Zhang, B. Ozdamar, A.A. Ogunjimi, E. Alexandrova, G.H. Thomsen, and J.L. Wrana. 2003. Regulation of cell polarity and protrusion

formation by targeting RhoA for degradation. *Science*. 302:1775–1779. doi:10.1126/science.1090772

Warner, S.J., and G.D. Longmore. 2009. Distinct functions for Rho1 in maintaining adherens junctions and apical tension in remodeling epithelia. *J. Cell Biol.* 185:1111–1125. doi:10.1083/jcb.200901029

Wilkinson, S., H.F. Paterson, and C.J. Marshall. 2005. Cdc42-MRCK and Rho-ROCK signalling cooperate in myosin phosphorylation and cell invasion. *Nat. Cell Biol.* 7:255–261. doi:10.1038/ncb1230

Yang, L., L. Wang, and Y. Zheng. 2006. Gene targeting of Cdc42 and Cdc42GAP affirms the critical involvement of Cdc42 in filopodia induction, directed migration, and proliferation in primary mouse embryonic fibroblasts. *Mol. Biol. Cell*. 17:4675–4685. doi:10.1091/mbc.E06-05-0466

Zhang, H., and I.G. Macara. 2008. The PAR-6 polarity protein regulates dendritic spine morphogenesis through p190 RhoGAP and the Rho GTPase. *Dev. Cell*. 14:216–226. doi:10.1016/j.devcel.2007.11.020